# Cells transplanted onto the surface of the glial scar reveal hidden potential for functional neural regeneration

AUTHOR(S):

Sekiya, Tetsuji; Holley, Matthew C.; Hashido, Kento; Ono, Kazuya; Shimomura, Koichiro; Horie, Rie T.; Hamaguchi, Kiyomi; Yoshida, Atsuhiro; Sakamoto, Tatsunori; Ito, Juichi

CITATION:

Sekiya, Tetsuji ...[et al]. Cells transplanted onto the surface of the glial scar reveal hidden potential for functional neural regeneration. Proceedings of the National Academy of Sciences 2015, 112(26): E3431-E3440

ISSUE DATE:

2015-06-15

URL:

http://hdl.handle.net/2433/198455

**Biological Sciences – Neuroscience**

# Cells transplanted onto the surface of the glial scar reveal hidden potential for functional neural regeneration

Short title: **Cell transplantation on glial scar**

**Tetsuji Sekiya[a,1], Matthew C. Holley[b], Kento Hashido[a], Kazuya Ono[a,*], Koichiro Shimomura[c], Rie T. Horie[a,†], Kiyomi Hamaguchi[a], Atsuhiro Yoshida[a], Tatsunori Sakamoto[a], Juichi Ito[a]**

[a]Department of Otolaryngology, Head and Neck Surgery, Kyoto University Graduate School of Medicine, Sakyou-ku, Kyoto, 606-8507 Japan, [b]Department of Biomedical Science, The University of Sheffield, Firth Court, Western Bank, Sheffield, S10 2TN England, [c]Graduate School of Agriculture, Kyoto University, Sakyou-ku, Kyoto, 606-8502 Japan.

Present addresses; *Laboratory of Molecular Biology, NIDCD, Porter Neuroscience Research Center, †Department of Biomaterials Field of Tissue Engineering, Institute for Frontier Medical Sciences, Kyoto University.

[1]To whom correspondence should be addressed. E-mail: tsekiya@ent.kuhp.kyoto-u.ac.jp
Tetsuji Sekiya, Department of Otolaryngology, Head and Neck Surgery, Kyoto University Graduate School of Medicine, Sakyou-ku, Kyoto, 606-8507 Japan.

The authors declare no competing financial interests and no conflict of interest.

Author contributions: T. Se designed experiments, performed all experiments except Western blotting, qRT-PCR and ELISA, prepared figures and wrote the manuscript. M.C.H. provided the donor cells (US/VOT-N33) and critically edited the manuscript. Ke. H., K.O. performed Western blotting studies. K. S. carried out qRT-PCR. R.T. H. supervised laboratory technicians. Ki. H., T. Sa provided reagents. A.Y. gave technical advice. J. I. supervised experiment.

**Abstract**

Cell transplantation therapy has long been investigated as a therapeutic intervention for neurodegenerative disorders, including spinal cord injury, Parkinson's disease and amyotrophic lateral sclerosis. Indeed, patients have high hopes for a cell-based therapy. However, there are numerous practical challenges for clinical translation. One major problem is that only very low numbers of donor cells survive and achieve functional integration into the host. Glial scar tissue in chronic neurodegenerative disorders strongly inhibits regeneration and this inhibition must be overcome to accomplish successful cell transplantation. Intra-neural cell transplantation is considered to be the best way to deliver cells to the host. We have questioned this view with experiments in vivo on a rat glial scar model of the auditory system. Our results show that intra-neural transplantation to the auditory nerve, preceded by chondroitinase ABC (ChABC)-treatment, is ineffective. There is no functional recovery and almost all transplanted cells die within a few weeks. However, when donor cells are placed on the surface of a ChABC-treated gliotic auditory nerve, they autonomously migrate into it and recapitulate glia- and neuron- guided cell migration modes to repair the auditory pathway and recover auditory function. "Surface transplantation" may thus pave the way for improved functional integration of donor cells into host tissue, providing a less invasive approach to rescue clinically important neural tracts.

**Key words:** Astrocyte, Auditory system, Cell transplantation, Glial scar, Neurodegenerative diseases

**Significance Statement**

Cell transplantation can restore function in neurodegenerative disorders but the low rate of functional integration of donor cells into host is a major limiting factor for clinical application. This is closely related to the long-standing view that donor cells must be transplanted intra-neurally. We show that glial scar, which is common in neurodegenerative conditions, inhibits the survival of intra-neurally transplanted cells in our rat glial scar model in the auditory system. However, cells placed on the "surface" of scar tissue autonomously enter the nerve and become functionally integrated into the host. The glial scar, normally considered to be a barrier to cell transplantation, includes important structural and chemical cues that are disrupted by intra-neural delivery but preserved by "surface transplantation".

¥body

Cells transplanted into the nervous system could cure various forms of neurodegenerative disease and neural injury (1, 2) but most donor cells die without functional integration (3) and glial scar tissue is strongly inhibitory to axon regeneration (4). Glial scar tissue forms following conditions such as ischemia or mechanical trauma when reactive astrocytes increase proliferation, become hypertrophic and up-regulate glial fibrillary acidic protein (GFAP) (5, 6). In this study, however, we demonstrate that if donor cells are delivered appropriately, they can interact successfully with the glial scar and restore lost neuronal function. We developed an in vivo model of the chronic gliotic environment in clinical patients by compressing the rat auditory nerve without breaching the fluid spaces that contain the sensory structures inside the cochlea (7-10). In this model, spiral ganglion cells (the auditory neurons) degenerate selectively but hair cells are preserved both morphologically and functionally (7, 8, 10, 11). We then waited 5 weeks before cell transplantation to allow the formation of a glial scar with the progressive degeneration of auditory neurons. We characterized the glial scar with several experimental measures. This is an important element because experimental models for cell-based therapies for neurodegenerative diseases should include the chronic gliotic environment to simulate the appropriate clinical condition in patients.

To compress the auditory nerve, the CNS portion was atraumatically exposed in the cerebellopontine angle cistern through right suboccipital craniectomy, a nerve hook was placed into the internal auditory meatus and the nerve was injured by a single compression **(Fig. 1A-B, S1A).** We used a murine auditory neuroblast cell line for transplantation (US/VOT-N33) (12). This cell line was derived from the ventral otocyst (inner ear anlage) of a mouse embryo at embryonic day ED10.5 and was selected because it expresses key markers for auditory sensory neurons and differentiates with the appropriate bipolar morphology in the ear both in vitro and in vivo (11, 12).

In the first experiments we delivered cells into the auditory nerve via a thin fused silica tube **(Fig. S1B),** treating the nerve topically with chondroitinase ABC (ChABC) (13) soaked in gelatin sponge at the time of nerve injury and then again immediately after cell transplantation. Three months later we assessed the structural and functional recovery of the auditory nerve.

During these experiments we noticed that donor cells that spilled onto the surface of the nerve were apparently able to enter the ChABC-treated tissue and to survive. Thus we reasoned that cell delivery onto the surface of the glial scar might be successful and less invasive. In this context we designed an experiment to compare two methods of cell delivery. In the first we applied the conventional method of intra-neural infusion and in

the second we delivered cells to the surface of the nerve without mechanical damage to its structure. We then compared the results in terms of cell morphology and functional recovery of the auditory system.

## Results

**An auditory system model of the glial scar.** The CNS portion of normal auditory nerve is relatively long compared with other cranial nerves and it projects into the auditory nerve trunk (14). The transitional zone between the PNS and the CNS lies within the temporal bone, distal to the internal auditory meatus **(Fig. 1A)** (15). It is defined by the boundary of the expression of GFAP, which is expressed only by the astrocytes in the CNS **(Fig. 1A-B left)**. Following compression, numerous changes occur that are characteristic of glial scar formation and that we confirmed in our model.

We first characterized the glial scar with antibodies to GFAP (6), which showed that compression in one ear led to thinning of the auditory nerve and extension of the GFAP domain peripherally **(Fig. 1B)**. Glial scar processes were observed to pass through Rosenthal's canal toward the habenula perforata through which the distal auditory neurons reach the hair cell regions **(Fig. 1C)**. Immunofluorescence for GFAP was increased relative to the sham ear **(Fig. 1D)**. The levels of GFAP protein in the compressed tissue were higher than in the sham operated ear **(Fig. 1E)** and the corresponding levels of mRNA expression were significantly higher after 1, 4 and 25 weeks **(Fig. 1F)**. Immunofluorescence and mRNA for neurocan, a class of chondroitin sulfate proteoglycans (CSPGs) that are predominantly produced by reactive astrocytes and that inhibit regeneration in the CNS (16), increased significantly **(Fig. 1G-H)**. Finally, mRNA for nestin, which is another hallmark of reactive gliosis (5, 6), increased significantly 4 weeks after compression **(Fig. 1I)** and nestin-positive glial scar processes were observed mainly at the compression site **(Fig. 1J)**. Treatment of compression-induced glial scars with ChABC was evaluated using the monoclonal antibody 2B6, which provides a measure of CSPG digestion (13). Five weeks after compression with ChABC treatment the antibody strongly labelled the scar, demonstrating effective digestion of CSPGs **(Fig. 1K)**.

**Functional recovery following cell transplantation.** In our animal surgery, the lateral part of the cerebellum was removed to fully expose the auditory nerve, inevitably resulting in a substantial change of bioelectric volume conductor around the auditory nervous system. Therefore, there was little value in comparing the ABR before surgery

with that after a large volume of the cerebellum was removed. Hence, we compared ABRs immediately before cell transplantation (5 weeks after auditory nerve compression) and 3 months after cell transplantation as there was no substantial volume change around auditory nervous system in these two stages.

There was no improvement in the auditory evoked brainstem responses (ABR) after 3 months in any of the 20 animals in which cells were delivered by intra-neural transplantation to ChABC-treated, gliotic auditory nerves (**Fig. 2A-C, S1B**). Positive, monophasic potentials ("cut end potentials" (17)) indicated that sound-induced electrical activity did not pass the transplantation site. However, ABRs improved in 10 of the 17 animals in which cells were delivered by surface transplantation **(Fig.2D-F; Fig. S1B)**. In the ABRs, waves I and II represent activity in the auditory nerve and cochlear nucleus, respectively (18) (**Fig. S2A-B**) but they were attenuated by the direct mechanical injury and glial scar formation (**Fig. S2C**). Thus we evaluated function by measuring wave III, which originates in the contralateral superior olivary complex (SOC), more central than the origins of wave I and II (**Fig. S2A**). Its amplitude reflects activity entering the SOC via the cochlear nucleus and auditory nerve. There were significant improvements in wave III amplitude and threshold (**Fig. 2D-H, Table S1A-B**). Latency analysis revealed that conduction velocity recovered in the 16 kHz region but not in the 4 and 8 kHz regions (**Fig. 2I, Table S1C**). This may be because the 16 kHz region was nearest to the transplantation site, allowing more time for myelination, so a similar recovery might have occurred at 4 and 8 kHz over a longer period. In the sham rats to which medium-soaked gelatin sponge and fibrin glue were placed on the nerve (n=5), no significant changes in the ABRs were observed 3 months later, indicating that spontaneous recovery did not occur 5 weeks after auditory nerve compression.

**Integration of donor cells to the auditory nerve.** We observed no evidence of significant cell survival or integration after 3 months in any of the 20 animals in which cells were delivered by intra-neural transplantation to ChABC-treated gliotic auditory nerves. Furthermore, there was clear evidence of cell debris from the donor cells within the nerve (**Fig. 3A-B**). In stark contrast, cells transplanted on the surface of the glial scar did not die but survived attached to the surface of the auditory nerve and the brainstem **(Fig. 3C-D)**. There was evidence that groups of at least 15-20 cells had entered the auditory nerve 3 months after cell transplantation **(Fig. 3E)**. In some cases the cells appeared to migrate into the nerve in a chain formation **(Fig. 3F-G)** or aligned within conduit-like structures in the glial scar **(Fig. 3H-I)**. Transplanted cells that entered the proximal portion of the glial scar appeared to be guided by hypertrophic astrocytic

processes and migrated distally within the scar **(Fig. 3J-M)**.

Inside the nerve, transplanted cells were closely associated with GFAP+ processes (**Fig. 4A-B**), reminiscent of glia-guided migration of newborn neurons in the developing cortex (19, 20). Astrocytes at the lesion appeared to lose their stellate morphology and to adopt overlapping, elongated morphologies (21) (**Fig. 4C**). Among them, the transplanted cells were often organized in chains within the elongated GFAP+ processes (**Fig. 4D-E**). This behavior resembles the rostral migratory stream (RMS) where neuroblasts migrate within a tube-like structure, ensheathed by specialized GFAP+ astrocytes (22, 23).

Neurons can use existing axons for guidance (24), which seemed to be reiterated in our study **(Fig. 4F)**. We found numerous donor cells attached to residual neurons (**Fig. 4G-H**) and with lengthy GFP+ projections **(Fig. 4I)**. Residual neurons seemed to provide a scaffold in the core of dense anisomorphic glial scar tissue where thick GFAP+ glial scar processes lost their longitudinal orientation (**Fig. 4J-M**).

**Synaptic connections at the proximal and distal ends of the auditory nerve**. The ABR results imply that cells transplanted to the nerve surface form synapses both with hair cells and with neurons in the cochlear nuclei in the hindbrain. Evidence for such connections has been shown previously in a sub-acute model of cell therapy in the auditory system (25). We observed bundles of neurites expressing eGFP in Rosenthal's canal to the habenula perforata (HP, foramina nervosa) (**Fig. 5**). More specifically, at the basal and perinuclear regions of inner hair cells we found eGFP labelling co-localized with punctate labelling for the glutamate receptor sub-units GluR2/3 (26) (**Fig. 6A**). This provides strong evidence for innervation of hair cells by projections from the donor cells, particularly because postsynaptic glutamate receptors do not survive loss of auditory afferent neurons without cell transplantation (27).

In our experimental model, the PVCN (posteroventral cochlear nucleus) is affected most, the DCN (dorsal cochlear nucleus) less and the AVCN (anteroventral cochlear nucleus) was not affected (8). Hence, to most clearly evaluate how the transplanted cells re-innervate cochlear nucleus cells, we chose to evaluate the PVCN. We observed GFP+ process projecting towards the CN **(Fig. 6B)** and in animals with improved ABRs, eGFP and synaptophysin were co-localized in significantly larger numbers of ovoid cells, which were probably globular bushy cells, than in those without ABR improvements (**Fig. 6C-D**). The survival of CN cells depends on input from auditory neurons, so the cochlear nucleus cells that received neurites from transplanted cells had probably survived as a result (28).

**Correlation between cell survival and functional recovery.** We saw no functional recovery or cell survival with intra-neural transplantation. With surface transplantation we observed recovery of the ABRs in 10 of 17 animals treated. In those 10 animals the number of detectable donor cells after 3 months was significantly higher than in the remaining 7 (**Fig. 7A-D**) but the residual numbers of endogenous spiral ganglion cells was similar (**Fig. 7E-F**). This result provides strong evidence that the transplanted cells contributed to the observed improvements of wave III amplitudes, thresholds and conduction velocity. It also reveals a striking difference between the two methods of cell delivery, with greater functional recovery being linked to the less invasive method of surface transplantation.

**Cues for inward migration of surface cells**. The cues that guide the migration of transplanted cells are unknown. However, in our model the hair cells remain intact (10) and they should provide a source of neurotrophins, notably BDNF and NT-3, which are indispensable for the maintenance and survival of auditory neurons (28). Correspondingly, auditory neurons express the relevant receptors, trkB and trkC, respectively (28). We found that BDNF concentrations were higher in ChABC-treated tissue **(Fig. 8A)** and that the transplanted cells expressed TrkB receptors **(Fig. 8B-E)**.

## Discussion

We show that in our auditory nerve model, cells delivered to the surface of ChABC-treated glial scars can migrate into the nerve, extend neuritic processes and form synaptic connections to their peripheral and central targets. This is associated with significant functional recovery of the auditory pathway. In contrast, cells delivered by intra-neural infusion die without either integration or functional recovery. Most experiments in cell transplantation and axon regeneration have been performed soon after injury and before the glial scar has developed (13, 29, 30). Our transplantation model is designed to reflect the clinical situation in terms of damage, glial scar formation and subsequent surgery. In this model, changing the degree of compression provides a wide range of reproducible nerve injury as observed in human neurodegenerative diseases.

Our results suggest that the glial scar contains critical structural and chemical cues that should be preserved during transplantation. Intra-neural delivery either destroys those cues or places the cells immediately into a hostile cellular environment that does not allow them to engage with the tissue. In human neurodegenerative diseases, pathological processes progress chronically but numerous axons remain functional even at advanced

stages (31). Infusion pressure and the infused cell mass during surgery may damage these residual neurons. Moreover, intra-neural damage may re-activate the process of glial scar formation again as observed in surgical removal of glial scar tissue (32). In contrast, surface delivery may enable cells to make appropriate adaptations to the tissue matrix to ensure that they survive once they migrate into the nerve. We show that BDNF could be an important guidance and survival factor in our model. The relatively higher survival rate (13.7%) of the transplanted cells in this experiment may have been due to the delivery site, where there were appropriate cues from the sensory epithelium and nutrients from the cerebrospinal fluid. The removal of CSPG side chains by ChABC might facilitate the diffusion of BDNF through the nerve from the hair cells (33) and the gradient might be preserved better without damage by intra-neural intervention. Nevertheless, there are many other soluble signaling molecules that could be important. Furthermore, there are numerous intercellular interactions, mediated by molecules such as N-cadherin and NCAM, which play a crucial role in regenerating and directing axons (34). In a study where dorsal root ganglion neurons were seeded onto organotypic slices containing the corpus callosum, the donor neurons regenerated lengthy axons along the processes of gliotic astrocytes, and fibronectin expressed on the surface of the astrocytes was an important factor for this regeneration (35). Intriguingly, donor cells appeared able to jump from one astrocytic process to another (35). Such cues are likely to be important for integration of transplanted cells in our model.

The structure of the scar is likely to be critical for the integration of transplanted cells. In our study, glial processes projected distally into the small bony canals beyond the fundus of the internal auditory canal and this phenomenon was observed equally in animals with and without ChABC treatment **(Fig. 1B right, 1C, 3A)**, indicating ChABC did not change the basic framework of the glial scar as far as we can judge from the GFAP immunohistochemistry. However, ChABC apparently aided the donor cells to efficiently exploit preserved positive cues because it digests glycosaminoglycan (GAG) chains of CSPGs and removes their inhibitory influence (36). GAG chains of CSPGs interact with inhibitory neuronal receptors, including receptor protein tyrosine phosphatase sigma (RPTPσ), leukocyte common antigen-related (LAR) phosphatase and Nogo receptors 1 and 3 (NgR1, 3), preventing axon regeneration (29, 30, 36). In addition to such receptor-mediated mechanisms, it was recently demonstrated that ChABC modifies the immuno-inflammatory process of the injured CNS (37, 38). Macrophages have two distinct polarized phenotypes, M1 and M2, depending on the local tissue environment (39). In the acute stage of spinal cord injury, pro-inflammatory M1 macrophages dominate the lesion but during the resolution stage they are replaced by anti-inflammatory M2 macrophages

(40). M2 macrophages produce anti-inflammatory cytokines including IL-10 (40) and several in vivo experimental studies indicate IL-10 promotes recovery after spinal cord injury (41, 42). Recently, it was demonstrated viral overexpression of ChABC induced anti-inflammatory M2 macrophage polarization (37) accompanied with increased expression of IL-10, resulting in reduced tissue loss in rat spinal cord injury (38).

Following spinal cord injury in amphibians and fish, glial (astrocytic) bridges span the injury site and guide neuritic growth, resulting in remarkable functional recovery (43). Experimentally, many cells, matrices and nerve grafts have been investigated as the bridge to fill the lesion in mammals (44). In this context, it is reported that immature astrocytes injected along with ChABC are capable of forming the bridge-building process beyond the gliotic lesion in the adult rat cingulum, probably through a matrix metalloproteinase-2 (MMP-2) dependent mechanism (44). In our study a “glial scar bridge” was effectively formed from endogenous astrocytes **(Fig. 1B right, 1C)**, which may have helped to guide donor cells and to support neurite elongation. In cell transplantation, the transition zone between the CNS and PNS **(Fig. 1A)** can be a significant barrier for cell migration and neurite extension (45). However, this may be overcome by the formation of glial scar bridge.

Neuron-guided cell migration may also be important. We observed residual neuronal elements in glial scar tissue that lacked parallel alignment of glial processes and these residual neurons were used by the donor cells as the scaffold **(Fig. 4J-M)**. Hence, delayed clearance of myelin debris, uniquely observed in CNS degeneration and regarded as an inhibitory factor for axon regeneration (46), is not necessarily disadvantageous for donor cells in cell transplantation therapy (35, 44). Taken together, transplanted cells seem to utilize complementary structural and chemical guidance cues from both neurons and glial cells, depending on the environment surrounding them (**Fig. 4**).

Survival, differentiation and integration of donor cells depend on their molecular programs and their ability to respond to the host environment (47). Our donor cells were region-restricted precursor cells at a relatively late stage of inner ear development (12). Precursor cells have numerous advantages over less committed, proliferating progenitors because precursors with defined transcription factors expressed at a specific ontogenetic stage have more chance to be integrated into the host than progenitor or stem cells that have not yet begun to express such factors (48).

Cell therapy for neuronal regeneration is an ambitious goal in restorative medicine and numerous practical steps must be addressed for effective clinical translation. In our experiments, the average improvement of ABR thresholds was about 10 dB SPL **(Fig. 2E-F, H)**, which is clinically relevant because serviceable function can be achieved with

a relatively small number of functional neurons. With only 5-10% of the total axonal population, patients with cochlear implant are able to hear (49). Coincidentally, a similar value of functional motor neurons can enable patients to become mobile (50). Thus, we believe that surface transplantation is a less invasive technique that could have more widespread application to the nervous system. In amyotrophic lateral sclerosis (ALS), anterior horn cells and axons often degenerate (51). Suitable donor cells applied on the surface of degenerated anterior roots of the spinal cord could provide a minimally invasive method of cell transplantation to restore lost function of the motor neurons. Similarly, surface transplantation of appropriate motor neuron precursors may ameliorate neurological deficit due to poliomyelitis in which anterior horn cells degenerate (52). Patients with neurological sequelae from peripheral neuropathy with spinal cord or brainstem involvements may also be candidates for surface transplantation (53). We demonstrated that elongated, astrocytic processes after trauma played a crucial role in cell migration **(Fig. 4A-E)** and intriguingly similar elongated processes in reactive astrocytes are observed in multiple sclerosis (54). Since we observed neurites from transplanted cells in the cochlear nucleus, surface transplantation may be applied not only to neural systems in the superficial layers of the nervous system but also to those in deeper locations. This could include the substantia nigra and the caudate nucleus, which may be approachable via cisternal and intraventricular routes.

In conclusion, the glial scar has been regarded as a major barrier for cell transplantation therapy but we show that this is not necessarily the case if donor cells are applied appropriately to the host with minimal tissue damage. Our method of surface transplantation potentially opens the way to more efficient and less invasive approaches for cell transplantation in many forms of CNS and PNS disorders.

## Materials and Methods

### Glial scar induction in rat auditory system by mechanical compression to auditory nerve.

Animal experiments were conducted in accordance with the Guidelines for Animal Experiments at Kyoto University. Exposing of the auditory nerve of male Sprague-Dawley rats (P7-8 weeks) was performed as previously reported (7, 8, 10, 11). For compression, a nerve hook (tip diameter: 0.15 mm, No. 10140-03, Fine Science Tools, Canada) with the tip bent at a 150-degree angle was placed onto the auditory nerve at the internal auditory meatus and the nerve was mechanically injured by a single compression (**Fig. S1A**).

**Cell transplantation**

To treat the nerve topically with enzyme we applied a piece of absorbable gelatin sponge (2.0 $mm^3$) (Spongel®, Astellas Pharma) soaked in 20μL (0.2U) of chondroitinase ABC (Seikagaku, Sigma-Aldrich), first at the time of nerve injury and second, immediately after cell transplantation. Five weeks after auditory nerve mechanical injury, we re-opened the operative site and inserted a fused silica tube (external and internal diameter, 105 μm and 40 μm, respectively, Eicom, Japan) into the auditory nerve trunk **(Fig. S1B)**. For surface transplantation, we placed a fused silica tube approximately 500 μm away from the surface of auditory nerve in the cerebellopontine angle cistern **(Fig. S1B)**. In both experiments, we applied another ChABC-soaked gelatin sponge and covered the site with fibrin glue (Beriplast-P Combi-set®, CSL Behring; Bolheal®, Kaketsuken). We then infused 17,500 ± 2,400 cells (average ± SD) in 2μL of high concentration Matrigel® (BD), with bFGF (Peprotech, 25 ng/mL) that aids cell differentiation (12), using a microinjector (Micro 4, World Precision Instruments) with an infusion speed of 1,000 nL/min. Valproic acid (Wako, Japan) was orally administered in drinking water (480 mg/kg body weight/day), to enhance neurite extension (55), from one week before cell transplantation until the day of perfusion/fixation for 18 weeks.

**Immunohistochemistry**

Temporal bones were obtained and processed as reported (7, 8, 10, 11). The section angle was chosen so that the auditory nerve trunk, posteroventral (PVCN) and dorsal cochlear nucleus (DCN) were simultaneously included in one section as fully as possible by reference to Fig. 1 and 2 in Hackney et al (56). Primary antibodies used in the current study are listed in **SI Methods and Fig. S1C**.

**Quantification of immunofluorescence intensity**

Images were obtained with identical confocal microscope and microscope settings throughout capturing of images; the fluorescence intensities of GFAP in sham and experimental samples were compared at the same threshold (n=4). In 1G2 and 2B6 antibodies, the fluorescence intensity in sham samples was manually reduced to approximately zero level and at this level the images of experimented specimens were photographed (n=4). Images were converted into grey scale images with Photoshop (CS3, Adobe), transferred to NIH Image J and positive pixel area (P.P.A.) was analysed applying the same threshold.

**Western blotting of GFAP**

Samples were collected from experimental rats, 4 weeks after compression (right side, n=19) and those from sham rats were used as control. After processing, proteins were separated on a SuperSep Ace gel (Wako) and transferred into PVDF membrane (GE Healthcare). Membranes were probed with GFAP antibody (1:15,000, Dako, rabbit polyclonal) overnight and horseradish peroxidase-linked anti-rabbit IgGs (1:10,000, GE Healthcare) were applied as the secondary antibody. GAPDH was used as a loading control. Detailed information is listed in **SI Methods.**

**qRT-PCR**

The samples were collected from the rats 1, 4, and 25 weeks after compression (15 rats for each time point). Total RNA was extracted using an RNeasy Mini Kit (Qiagen). Single-stranded cDNA was synthesized with a High Capacity cDNA synthesis kit (Applied Biosystems). Real-time PCR primers and probes were obtained from Applied Biosystems (CSPG3, Neurocan, Rn00581331_m1; GFAP, Rn00566603_m1; Nestin, Rn00564394_m1). The data were acquired in triplicate. Gene expression values, normalized to GAPDH expression, were determined by using the comparative Ct method (ΔΔCt method). Detailed information is listed in **SI Methods.**

**ELISA**

Samples collected from 30 rats (5-10 weeks after compression) were processed after Elfving et al (57). ELISA study was performed with a Promega BDNF Emax ImmunoAssay System following the manufacturer's instructions. Detailed information is listed in **SI Methods.**

**Counting of spiral ganglion cells, transplanted cells and cochlear nucleus cells**

In 4 sham rats, 6 rats with ABR improvement and 4 rats without ABR improvement, we counted the numbers of spiral ganglion cells with nuclei in Rosenthal's canal in the basal cochlear turn (approximately corresponds to 70-100% of entire cochlear length from the cochlear apex), middle turn (70-30%) and apical turn (-30%) (58) in every 4th section in each rat. In the latter 2 groups of the rats, GFP+ transplanted cells were counted. For quantification of cochlear nucleus cells, we chose a section that included auditory nerve root, PVCN and DCN most widely among the sections and counted cells with synaptophysin+ endbulbs in sham rats and those with GFP+ synaptophysin+ endbulbs in experimental rats, in 5 randomly selected regions that approximately evenly covered entire PVCN (each region size, 270 x 270 μm) in each animal (5 rats with ABR

improvement; 4 rats without ABR improvement).

**ABR recording**

We recorded tone burst ABR three times in each animal, before auditory nerve injury, 5 weeks after nerve injury before cell transplantation and 3 months after cell transplantation as previously reported (59). White noise (40 dB) was applied to the contralateral ear to prevent the contribution from non-tested ear. We measured wave III amplitude as shown in **Fig. S2C** at 85 dB SPL in 8 and 16 kHz and 75 dB in 4 kHz to avoid large cochlear microphonics in 85 dB in this frequency.

**Statistical analysis**

Unpaired or paired Student's two-tailed t-test was performed using Excel 2013 (Microsoft). For all statistical tests $P<0.05$ was used as the criterion for statistical significance. In all figures, error bars indicate one standard deviation.

**Acknowledgements**

This work was supported by grants from Japan Society for the Promotion of Science, Univers Foundation, The General Insurance Association of Japan, the Japan Health Foundation, Osaka Gas Group Welfare Foundation, ZENKYOREN and Mitsui Sumitomo Insurance Welfare Foundation. An immunosuppressant FK-506 was gifted from Astellas Pharma Inc. Tokyo, Japan for the preliminary experiment of this study.

**References**

1. Bjorklund A, Stenevi U, Schmidt RH, Dunnett SB, & Gage FH (1983) Intracerebral grafting of neuronal cell suspensions. II. Survival and growth of nigral cell suspensions implanted in different brain sites. *Acta Physiol. Scand. Suppl.* 522:9-18.
2. Kang X, *et al.* (2014) Dopamine release from transplanted neural stem cells in Parkinsonian rat striatum in vivo. *Proc. Natl. Acad. Sci. U. S. A.* 111(44):15804-15809.
3. Cregg JM, *et al.* (2014) Functional regeneration beyond the glial scar. *Exp. Neurol.* 253:197-207.
4. Silver J & Miller JH (2004) Regeneration beyond the glial scar. *Nat. Rev. Neurosci.* 5(2):146-156.
5. Buffo A, *et al.* (2008) Origin and progeny of reactive gliosis: A source of

multipotent cells in the injured brain. *Proc. Natl. Acad. Sci. U. S. A.* 105(9):3581-3586.

6. Pekny M & Lane EB (2007) Intermediate filaments and stress. *Exp. Cell Res.* 313(10):2244-2254.
7. Sekiya T, *et al.* (2011) Mechanical stress-induced reactive gliosis in the auditory nerve and cochlear nucleus. *J. Neurosurg.* 114(2):414-425.
8. Sekiya T, *et al.* (2012) Trauma-specific insults to the cochlear nucleus in the rat. *J. Neurosci. Res.* 90(10):1924-1931.
9. Forge A & Wright T (2002) The molecular architecture of the inner ear. *Br. Med. Bull.* 63:5-24.
10. Matsumoto M, Sekiya T, Kojima K, & Ito J (2008) An animal experimental model of auditory neuropathy induced in rats by auditory nerve compression. *Exp. Neurol.* 210(1):248-256.
11. Sekiya T, *et al.* (2007) Transplantation of conditionally immortal auditory neuroblasts to the auditory nerve. *Eur. J. Neurosci.* 25(8):2307-2318.
12. Nicholl AJ, *et al.* (2005) Differentiation of an auditory neuronal cell line suitable for cell transplantation. *Eur. J. Neurosci.* 22(2):343-353.
13. Bradbury EJ, *et al.* (2002) Chondroitinase ABC promotes functional recovery after spinal cord injury. *Nature* 416(6881):636-640.
14. Tarlov I (1937) Structure of the nerve root. II. Differentiation of sensory from motor roots; observations on identification of function in roots of mixed cranial nerves. *Arch. Neurol. Psychiatry* 37:1338-1355.
15. Fraher JP & Delanty FJ (1987) The development of the central-peripheral transitional zone of the rat cochlear nerve. A light microscopic study. *J. Anat.* 155:109-118.
16. Asher RA, *et al.* (2000) Neurocan is upregulated in injured brain and in cytokine-treated astrocytes. *J. Neurosci.* 20(7):2427-2438.
17. Moller AR (2011) Generation of Electrical Activity in the Nervous System and Muscles. *Neurophysiological Monitoring*, (Springer, New York), pp 23-41.
18. Shaw NA (1988) The auditory evoked potential in the rat - a review. *Prog. Neurobiol.* 31(1):19-45.
19. Rakic P (1990) Principles of neural cell migration. *Experientia* 46(9):882-891.
20. Marin O & Rubenstein JL (2003) Cell migration in the forebrain. *Annu. Rev. Neurosci.* 26:441-483.
21. Wanner IB, *et al.* (2013) Glial scar borders are formed by newly proliferated, elongated astrocytes that interact to corral inflammatory and fibrotic cells via

STAT3-dependent mechanisms after spinal cord injury. *J. Neurosci.* 33(31):12870-12886.

22. Lois C, Garcia-Verdugo JM, & Alvarez-Buylla A (1996) Chain migration of neuronal precursors. *Science* 271(5251):978-981.
23. Ghashghaei HT, Lai C, & Anton ES (2007) Neuronal migration in the adult brain: are we there yet? *Nat. Rev. Neurosci.* 8(2):141-151.
24. Schwanzel-Fukuda M & Pfaff DW (1989) Origin of luteinizing hormone-releasing hormone neurons. *Nature* 338(6211):161-164.
25. Chen W, *et al.* (2012) Restoration of auditory evoked responses by human ES-cell-derived otic progenitors. *Nature* 490(7419):278-282.
26. Ruel J, *et al.* (2007) Physiology, pharmacology and plasticity at the inner hair cell synaptic complex. *Hear. Res.* 227(1-2):19-27.
27. Yuan Y, *et al.* (2014) Ouabain-induced cochlear nerve degeneration: synaptic loss and plasticity in a mouse model of auditory neuropathy. *Journal of the Association for Research in Otolaryngology : JARO* 15(1):31-43.
28. Rubel EW & Fritzsch B (2002) Auditory system development: primary auditory neurons and their targets. *Annu. Rev. Neurosci.* 25:51-101.
29. Shen Y, *et al.* (2009) PTPsigma is a receptor for chondroitin sulfate proteoglycan, an inhibitor of neural regeneration. *Science* 326(5952):592-596.
30. Dickendesher TL, *et al.* (2012) NgR1 and NgR3 are receptors for chondroitin sulfate proteoglycans. *Nat. Neurosci.* 15(5):703-712.
31. Brown JM, Vivio N, & Sheean GL (2012) The clinical practice of reconstructive neurosurgery. *Clin. Neurol. Neurosurg.* 114(5):506-514.
32. Lu P, Jones LL, & Tuszynski MH (2007) Axon regeneration through scars and into sites of chronic spinal cord injury. *Exp. Neurol.* 203(1):8-21.
33. Tropea D, Caleo M, & Maffei L (2003) Synergistic effects of brain-derived neurotrophic factor and chondroitinase ABC on retinal fiber sprouting after denervation of the superior colliculus in adult rats. *J. Neurosci.* 23(18):7034-7044.
34. Skaper SD (2005) Neuronal growth-promoting and inhibitory cues in neuroprotection and neuroregeneration. *Ann. N. Y. Acad. Sci.* 1053:376-385.
35. Tom VJ, Doller CM, Malouf AT, & Silver J (2004) Astrocyte-associated fibronectin is critical for axonal regeneration in adult white matter. *J. Neurosci.* 24(42):9282-9290.
36. Chien PN & Ryu SE (2013) Protein tyrosine phosphatase σ in proteoglycan-mediated neural regeneration regulation. *Mol. Neurobiol.* 47(1):220-227.
37. Bartus K, *et al.* (2014) Large-scale chondroitin sulfate proteoglycan digestion

with chondroitinase gene therapy leads to reduced pathology and modulates macrophage phenotype following spinal cord contusion injury. *J. Neurosci.* 34(14):4822-4836.

38. Didangelos A, Iberl M, Vinsland E, Bartus K, & Bradbury EJ (2014) Regulation of IL-10 by chondroitinase ABC promotes a distinct immune response following spinal cord injury. *J. Neurosci.* 34(49):16424-16432.
39. Mantovani A, Sozzani S, Locati M, Allavena P, & Sica A (2002) Macrophage polarization: tumor-associated macrophages as a paradigm for polarized M2 mononuclear phagocytes. *Trends Immunol.* 23(11):549-555.
40. Kigerl KA, *et al.* (2009) Identification of two distinct macrophage subsets with divergent effects causing either neurotoxicity or regeneration in the injured mouse spinal cord. *J. Neurosci.* 29(43):13435-13444.
41. Knoblach SM & Faden AI (1998) Interleukin-10 improves outcome and alters proinflammatory cytokine expression after experimental traumatic brain injury. *Exp. Neurol.* 153(1):143-151.
42. Zhou Z, Peng X, Insolera R, Fink DJ, & Mata M (2009) IL-10 promotes neuronal survival following spinal cord injury. *Exp. Neurol.* 220(1):183-190.
43. Goldshmit Y, *et al.* (2012) Fgf-dependent glial cell bridges facilitate spinal cord regeneration in zebrafish. *J. Neurosci.* 32(22):7477-7492.
44. Filous AR, *et al.* (2010) Immature astrocytes promote CNS axonal regeneration when combined with chondroitinase ABC. *Dev. Neurobiol.* 70(12):826-841.
45. Fraher JP (1999) The transitional zone and CNS regeneration. *J. Anat.* 194(Pt 2):161-182.
46. Filbin MT (2003) Myelin-associated inhibitors of axonal regeneration in the adult mammalian CNS. *Nat. Rev. Neurosci.* 4(9):703-713.
47. Kauhausen J, Thompson LH, & Parish CL (2013) Cell intrinsic and extrinsic factors contribute to enhance neural circuit reconstruction following transplantation in Parkinsonian mice. *J. Physiol.* 591(1):77-91.
48. MacLaren RE, *et al.* (2006) Retinal repair by transplantation of photoreceptor precursors. *Nature* 444(7116):203-207.
49. Khan AM, *et al.* (2005) Is word recognition correlated with the number of surviving spiral ganglion cells and electrode insertion depth in human subjects with cochlear implants? *Laryngoscope* 115(4):672-677.
50. Blight AR (1983) Cellular morphology of chronic spinal cord injury in the cat: analysis of myelinated axons by line-sampling. *Neuroscience* 10(2):521-543.
51. Moloney EB, de Winter F, & Verhaagen J (2014) ALS as a distal axonopathy:

molecular mechanisms affecting neuromuscular junction stability in the presymptomatic stages of the disease. *Front. Neurosci.* 8:252.

52. Howard RS (2005) Poliomyelitis and the postpolio syndrome. *BMJ* 330(7503):1314-1318.
53. Vucic S, Kiernan MC, & Cornblath DR (2009) Guillain-Barré syndrome: An update. *J. Clin. Neurosci.* 16(6):733-741.
54. Moreels M, Vandenabeele F, Dumont D, Robben J, & Lambrichts I (2008) Alpha-smooth muscle actin (alpha-SMA) and nestin expression in reactive astrocytes in multiple sclerosis lesions: potential regulatory role of transforming growth factor-beta 1 (TGF-beta1). *Neuropathol. Appl. Neurobiol.* 34(5):532-546.
55. Yuan PX, *et al.* (2001) The mood stabilizer valproic acid activates mitogen-activated protein kinases and promotes neurite growth. *J. Biol. Chem.* 276(34):31674-31683.
56. Hackney CM, Osen KK, & Kolston J (1990) Anatomy of the cochlear nuclear complex of guinea pig. *Anat. Embryol. (Berl.)* 182(2):123-149.
57. Elfving B, Plougmann PH, & Wegener G (2010) Detection of brain-derived neurotrophic factor (BDNF) in rat blood and brain preparations using ELISA: pitfalls and solutions. *J. Neurosci. Methods* 187(1):73-77.
58. Viberg A & Canlon B (2004) The guide to plotting a cochleogram. *Hear. Res.* 197(1-2):1-10.
59. Shiga A, *et al.* (2005) Aging effects on vestibulo-ocular responses in C57BL/6 mice: comparison with alteration in auditory function. *Audiol. Neurootol.* 10(2):97-104.

## Figure legends

**Figure 1. Glial scar formation after auditory nerve compression.** (A) The CNS portion (CNS-P) of the normal auditory nerve protrudes into the auditory nerve trunk and the transitional zone (TZ) at the boundary with the PNS is within the internal auditory canal (IAC). Mechanical compression (red arrow) applied to the CNS-P induced a glial scar. The red circle corresponds to that in Fig. S1A. BS, brainstem; CN, cochlear nucleus; Fs, fundus of the internal auditory canal; HC, hair cell; HP, habenula perforata; IAM, internal auditory meatus; PNS-P, PNS portion of the auditory nerve; SGC, spiral ganglion cells. (B) Auditory nerve (AuN) in sham operated and compressed (Comp) ears. The compression site is marked with a double-arrow. Distal extension of the GFAP domain is indicated by arrowheads. Spiral ganglion cells, labeled with Tuj1, were lost following

compression (multiple single arrows). Asterisks indicate glial scar processes projecting into small bony canals beyond the fundus of the IAC. (C) Fluorescence image of glial scar formed 5 weeks after auditory nerve injury, ChABC-treated (upper panels). The boxed area is enlarged in lower panels where confocal microscopy disclosed fine glial scar processes (arrowheads) past Rosenthal's canal (R). The margin of the limbus was non-specifically stained (arrows). bsl, mdl, ap - basal, middle, apical cochlear turn, respectively. (D) Expression of GFAP. PPA, positive pixel area (n=4). (E) Western blot for GFAP. (F) Relative expression of GFAP mRNA after 1, 4 and 25 weeks. (G) Expression of 1G2 (Neurocan) (n=4). (H) Relative expression of Neurocan mRNA. (I) Relative expression of Nestin mRNA. (J) Nestin expression at compression site. Most of the glial scar processes were Nestin-positive (arrowheads) and some were GFAP-positive (arrows). The boxed area in the left panel is enlarged in the right. The asterisk indicates tissue loss due to compression injury. (K) The ChABC-digested auditory nerve was 2B6-positive (n=4). Scale bars, 200 μm in B, C upper, 100 μm in J, 20 μm in C lower, D, G, K. All values represent mean ± SD. *p<0.05, **p<0.01, ***p<0.001.

**Figure 2. Recovery of ABRs after intra-neural and surface transplantation of cells.** A-C: Auditory evoked brainstem responses (ABRs) before compression (A), 5 weeks after compression before cell transplantation (B) and 3 months after intra-neural cell transplantation (C). Arrowhead in C, monophasic positive potential indicating electrical failure of nerve impulse transmission. D-F: ABRs before compression (D), 5 weeks after compression (E), and 3 months after surface transplantation (F). G-I: Amplitudes (G) and threshold values (H) of wave III, before (blue) and 3 months after cell transplantation (red). (I) Latency of wave III before and after cell transplantation (n=10).

**Figure 3. Donor cells after intra-neural (A-B) and surface delivery (C-M).**
(A) Intra-neurally transplanted cells died within 2 months of transplantation and cell debris (arrows) was found scattered within the nerve, mainly in the site of delivery (oblique bar). Arrowheads indicate glial scar processes projecting into small bony canals beyond the fundus of the internal auditory canal. AuN, auditory nerve. (B) GFP+ Tuj1+ cell debris was observed (arrows) within the cavity (*) formed after compression injury. (C-D) Layers of transplanted cells (arrows) were attached to the surface (dotted line) of the auditory nerve (AuN) (C) and brainstem (BS) (D). (E) A group of cells (arrowhead and arrows) inside the auditory nerve 3 months after cell transplantation. (F-G) Chains of donor cells (arrows) entered the auditory nerve from its surface (dotted lines) and others were aligned within a conduit-like structure in the glial scar (H-I). The arrowed area in H

is enlarged in I. (J) In the proximal portion of the glial scar (rectangle 1), transplanted cells (arrows in K) were loosely surrounded by hypertrophic, astrocytic processes (arrowheads in K) and apparently continued to migrate distally within the scar (rectangle 2 in J, L). Boxed areas 1 and 2 in J are enlarged in following panels K and L, respectively. Arrowhead in L indicates a cell outside the nerve. Oblique bar in J indicates the site of compression. (M) GFP+ transplanted cells (arrows) were abundant as observed in L. L and M are approximately adjacent sections. Scale bars, 200 μm in A, H, J, 50 μm in B, 25μm in C, 20 μm in F, I, D, E, M, L, 10 μm in K.

**Figure 4. Glia- and neuron-guided migration of transplanted cells.** (A, B) Transplanted cell (arrows) intimately related to GFAP+ process (arrowheads). (C) Transplanted cells among elongated glial scar processes. The boxed area is enlarged in (D-E). # - cavities at the compression epicenter, * - dead cells embedded into glial scar tissue. (D, E) Bipolar cells (arrows) formed chains within GFAP+ sheaths (arrowheads). (F) GFP+ Tuj1+ cell (arrow) attached to residual neurons (arrowheads). (G) The glial scar spread throughout the auditory nerve. The boxed area is enlarged in (H-I). (H) Transplanted cells (*) appeared to use neurons (arrowheads) for guidance. (I) GFP+ cells (arrows) in approximately the same area as in H. Arrowheads indicate GFP+ processes and triple arrows in left upper corner bipolar processes. (J-L) A gliotic area in auditory nerve (Boxed in J) is enlarged in K-L. One residual neuron (arrowheads in K, L) in a region of dense anisomorphic glial scar was apparently used by a transplanted cell (arrow in L) as the guide. Confocal imaging (L) disclosed a cell that was not identified by fluorescence microscopy (circle in K). Asterisks, tissue loss due to mechanical compression. (M) GFP+ cells (arrows) attached to Tuj1+ residual axon (arrowheads) in tandem. M is several sections apart from L, and roughly corresponds to upper part of L. Scale bars, 200 μm in G, J, 100 μm in C, 25 μm in F, 20 μm in A, H, I, 15 μm in K, L, M, 10 μm in D, E, 8 μm in B.

**Figure 5. Regenerating neurites in Rosenthal canal.** Bundle of GFP+ Tuj1+ neurites (arrowheads) projecting through Rosenthal's canal (R) to the habenula perforata (#). bsl, basal cochlear turn, OSL, osseous spiral lamina. Scale bars, 150 μm in left, 50 μm in right.

**Figure 6. Distal and proximal synaptic formations of the transplanted cells.** (A) Co-localization of label for GFP and GluR2/3 at the base and perinuclear region of an inner hair cell (arrowheads). The asterisk indicates a GluR2/3+ spot expressed perinuclearly. The dotted line indicates an inner hair cell. ap, apical cochlear turn, mdl, middle cochlear

turn. The boxed area shows location of adjacent panels. (B) Multiple GFP+ neurites in the brainstem (arrows), including one (double arrows) that reached a CN cell with co-localization of synaptophysin. (C) GFP+ synaptophysin+ cells (arrows) in rats with improved ABRs. Their morphology is reminiscent of endbulbs of the auditory nerve. The arrow in the left panel indicates the anterior direction. The small circle with the arrowhead in the left panel in B and C is the approximate location in the posteroventral cochlear nucleus (PVCN) that is enlarged in the following panels. Dotted lines in B and C indicate the surface of the brainstem. (D) Number of GFP+ synaptophysin+ cells in rats with and without ABR improvement in the PVCN (5 rats with ABR improvement; 4 rats without ABR improvement). AuN, auditory nerve, BS, brainstem. ** $p < 0.01$. Scale bars, 400 μm in left in B, C, 200 μm in left in A, 10 μm in right in A, B, C.

**Figure 7. Numbers of surface transplanted cells and spiral ganglion cells (SGC) in rats with and without ABR improvement.** (A-C) Three months after cell transplantation, donor cells were abundant within the auditory nerve trunk (arrowheads in A, B), and at the fundus and along the wall of the internal auditory canal (IAC) (arrowheads in C) in rats with improved ABRs. These cells aggregated as observed in Rosenthal's canal (areas 1, 2 in C). The boxed areas in A-C are enlarged in each adjacent panel. The dotted line in C is the fundus and wall of the IAC. (D) The number of eGFP+ transplanted cells was significantly larger in the rats with improved ABRs than in those without. The survival rate of transplanted cells in the rats with ABR improvement was 13.7% of total transplanted cells. (E) Residual spiral ganglion cells in basal, middle, and apical cochlear turns of sham treated and treated rats without ABR improvement are shown. Arrows indicate residual spiral ganglion cells in middle cochlear turns. (F) There was no significant difference in the residual numbers of endogenous SGCs between the rats with and without improved ABRs. Approximately 83-87% of SGCs degenerated after auditory nerve injury. The data is from 4 sham-operated rats, 6 rats with ABR improvement and 4 rats without ABR improvement. AuN, auditory nerve. Scale bars, 500 μm in left panels of A-C, 50 μm in right panels of C, E, 40 μm in right panels of A, B. *$p<0.05$, ***$p<0.01$, ****$p<0.001$.

**Figure 8. ELISA of ChABC-treated and untreated auditory system after compression and entry of donor cells from the surface of the auditory nerve.** (A) Significantly higher concentration of BDNF in ChABC-treated samples (Comp + ChABC) relative to untreated samples (Comp). **$p<0.01$. (B-E) GFP+ transplanted cells (arrows) entering the auditory nerve (AuN) from the surface (dotted lines) were TrkB-

positive. The boxed area in B is enlarged in C-E. Scale bars, 100 μm in B, 20 μm in D.

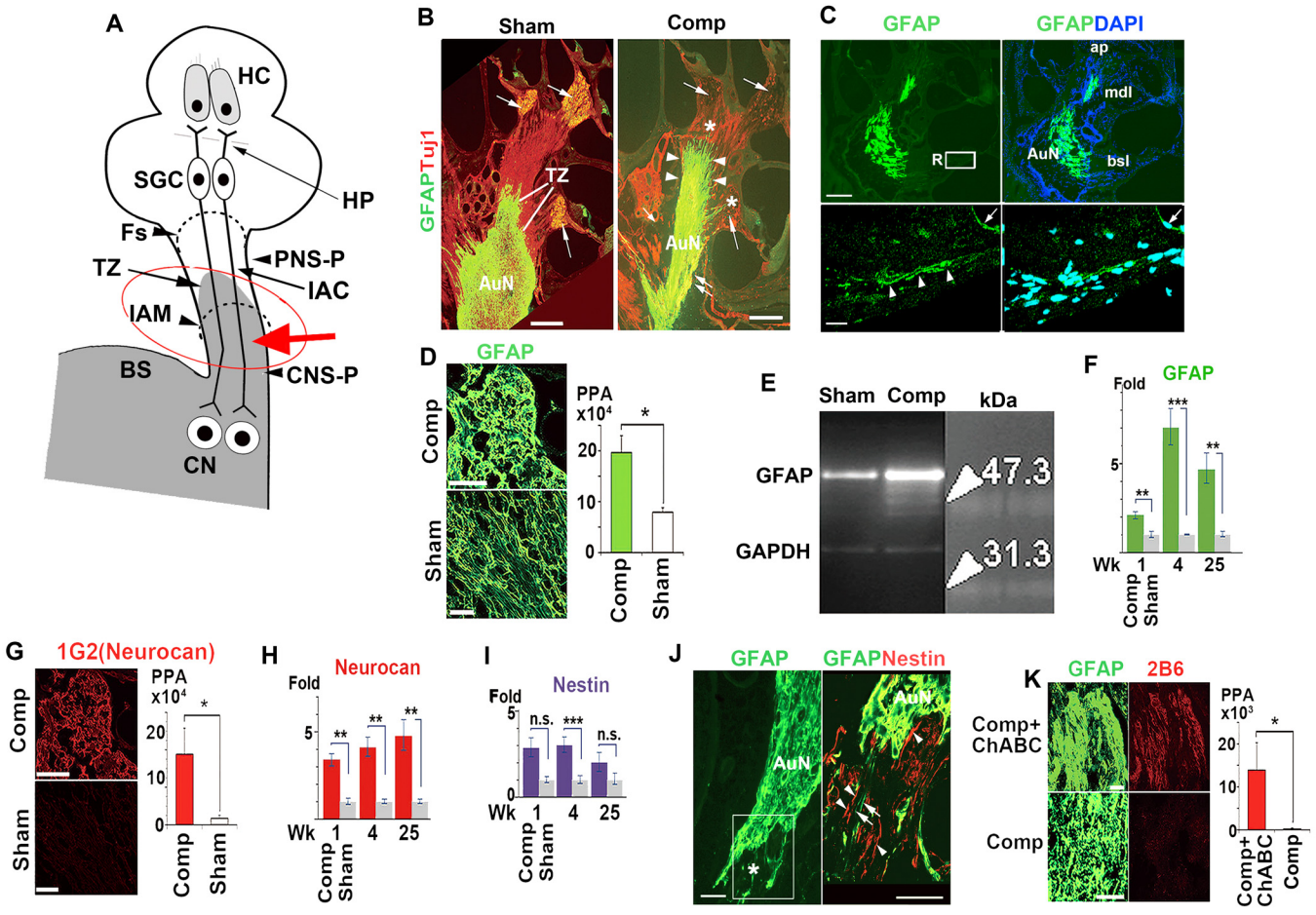


Figure 1

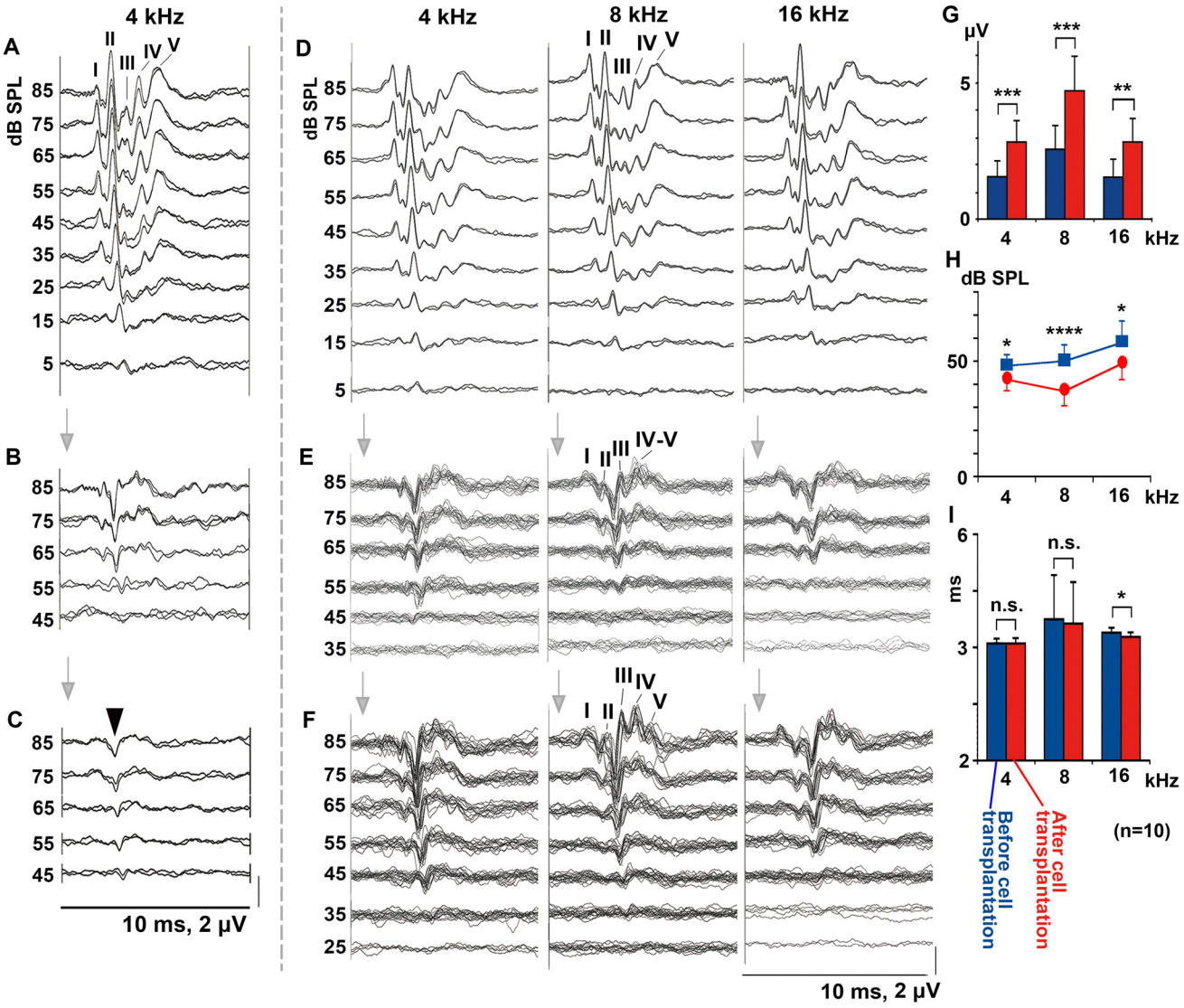


Figure 2

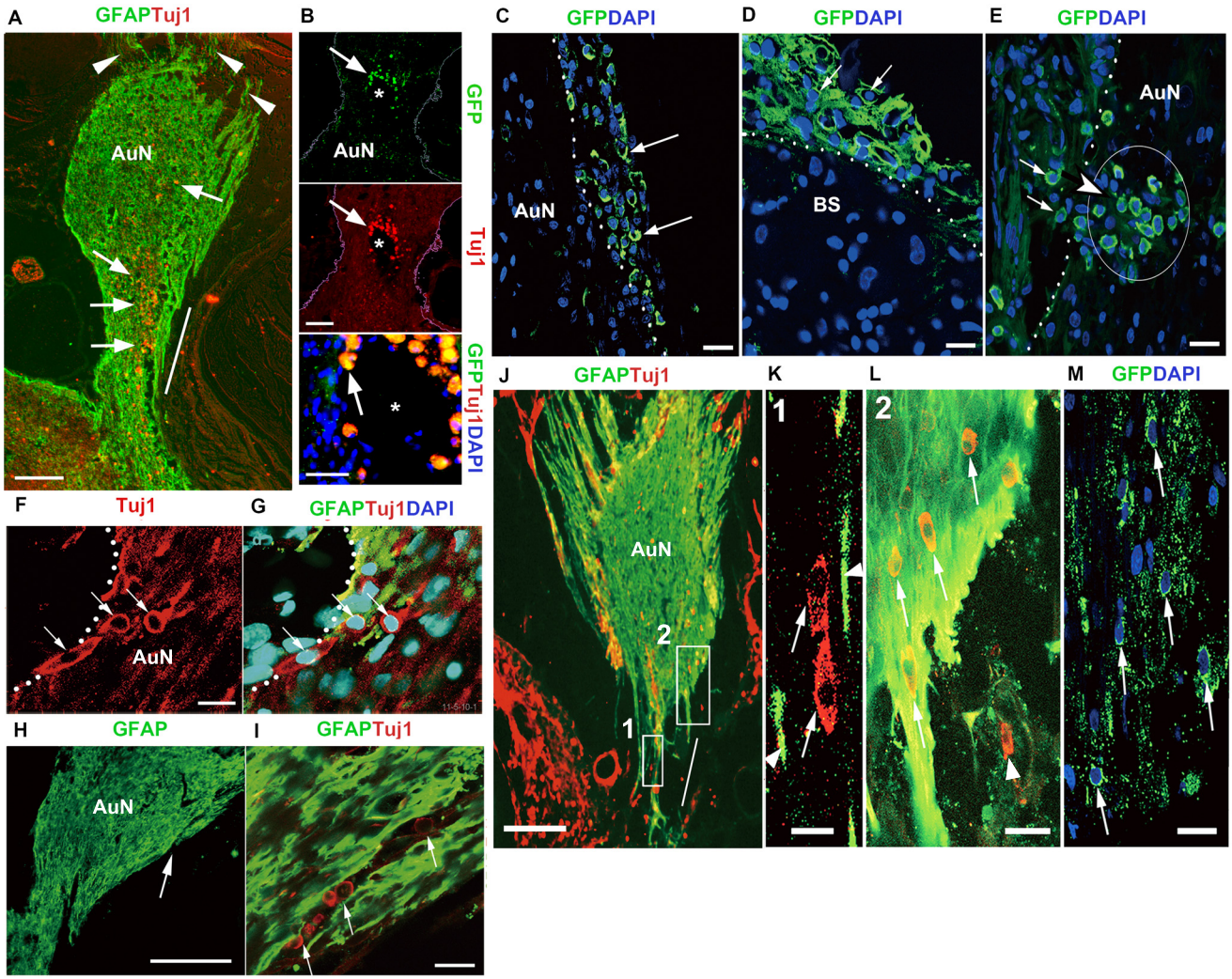


Figure 3

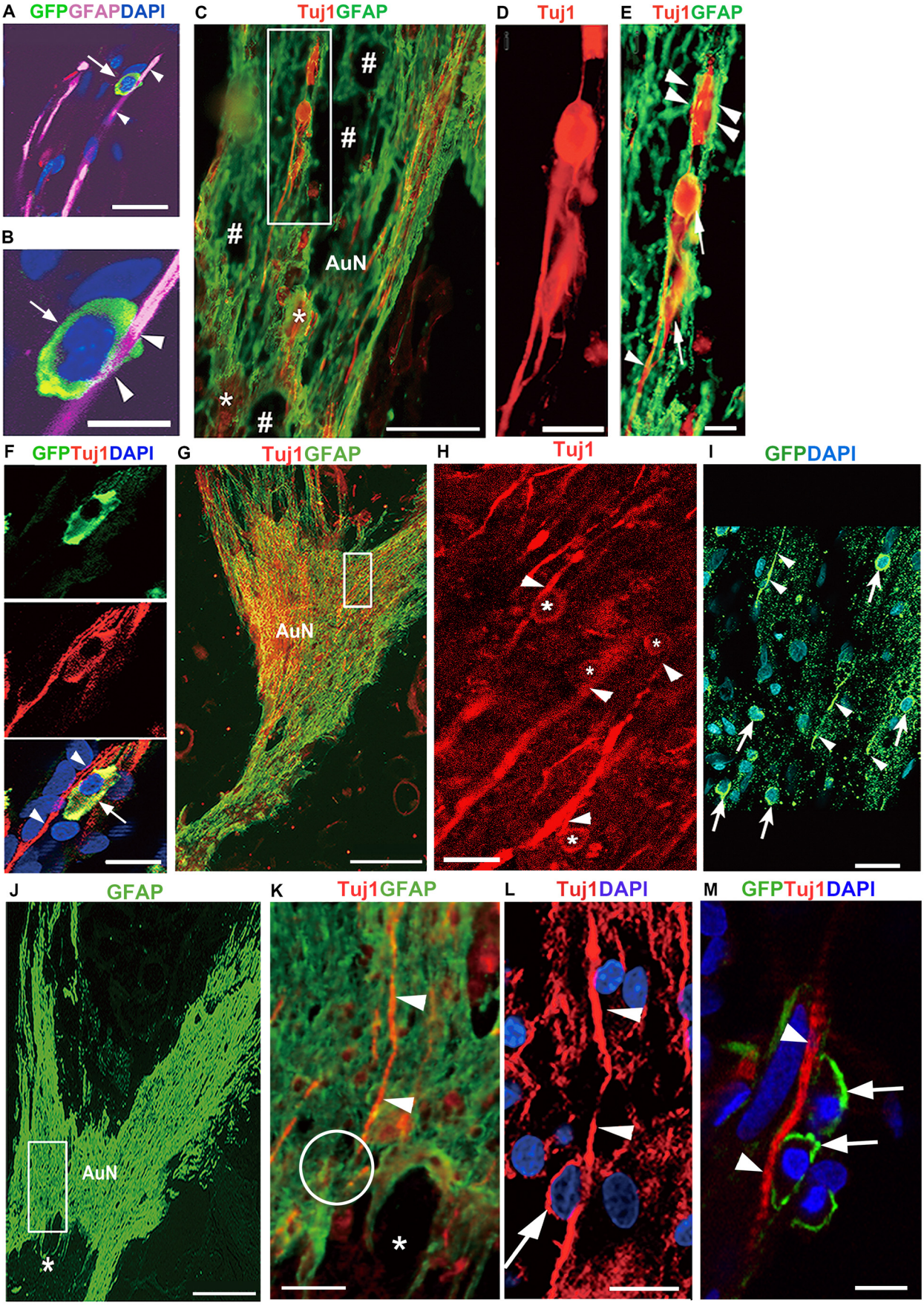


Figure 4

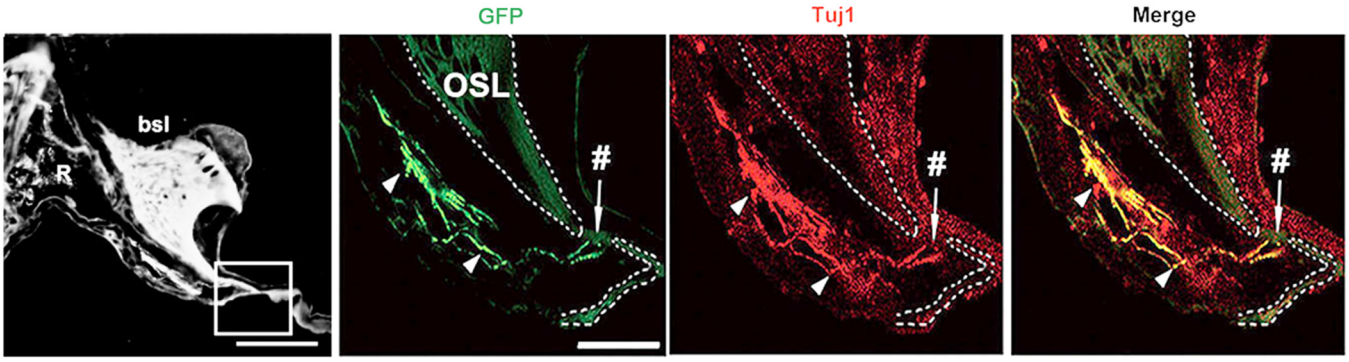


Figure 5

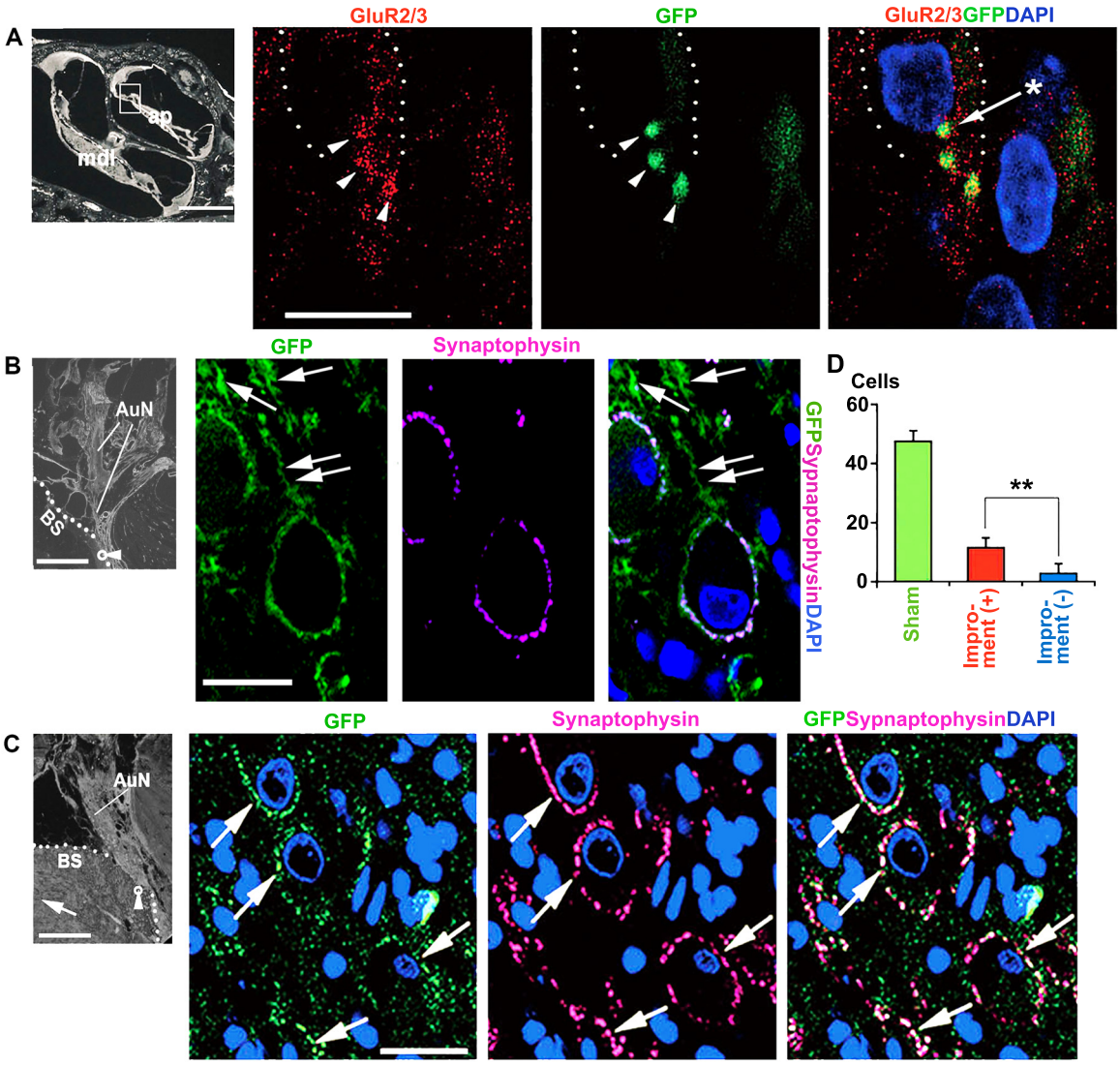


Figure 6

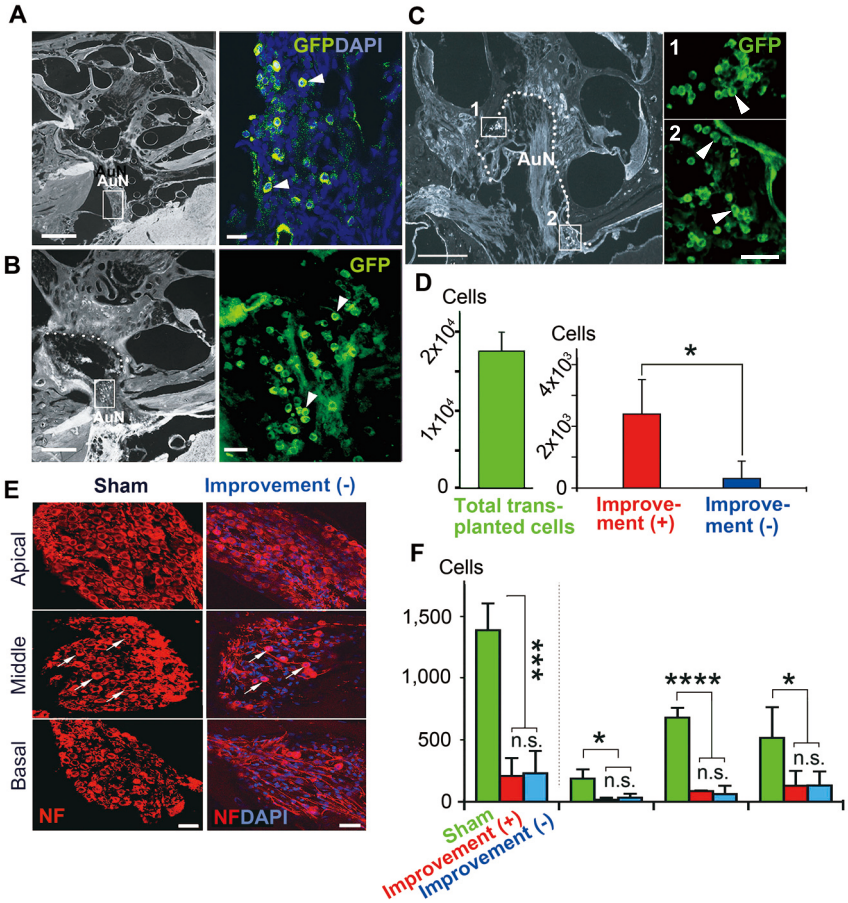


Figure 7

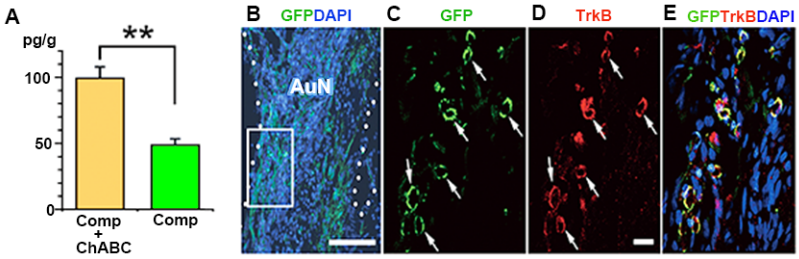


Figure 8

## Supporting Information Methods

### Immunohistochemistry

Temporal bones were decalcified with 10% ethylenediaminetetraacetic acid (EDTA) and HCl solution (pH 7.4) at 30°C for 5 weeks using a microwave processor (MI-33, Azumaya corporation, Japan). Serial 15 μm frozen sections were made by a cryostat (Leica CM1850, Leica Biosystems) after embedding into OCT compound. After blocking in the mixture of 10% normal goat serum (NGS) in PBS and 2% bovine serum albumin in PBS, sections were incubated in primary antibody diluted in 10% NGS overnight at 4°C. The targets of the following primary antibodies are as follows (Fig. S1C); anti-EGFP rabbit serum (1:500; Molecular Probes), anti-GFP rat monoclonal antibody (1:10,000, Nakalai tesque), anti-GluR 2/3 rabbit polyclonal (1:100, Millipore), anti-synaptophysin mouse monoclonal (1:100, BD Transduction laboratories), anti-beta III-tubulin mouse monoclonal antibody (Tuj1, 1:500, Covance Research Product), anti-neurofilament (NF) chicken polyclonal antibody (1:500 or 1000, Chemicon), anti-GFAP rabbit polyclonal antibody (1:500; DAKO), anti-neurocan mouse monoclonal antibody (1G2, 1:500, Seikagaku), anti-TrkB rabbit polyclonal (sc-12, 1:500, Santa Cruz Biotechnology), anti-nestin mouse antibody (1:500, BD Pharminogen), mouse monoclonal 2B6 antibodies (1:500, Seikagaku) and anti-myosin 7a rabbit polyclonal (1:500, Proteus Biosciences). The next day, the sections were washed extensively with PBS and incubated in the appropriate secondary antibodies, Alexa Fluor 488, 546, 568, 633 (1:500, Molecular Probes) and Cy3-conjugated IgG (1:500, Jackson Immunoresearch Laboratories). For nuclear staining, 4',6-diamidino-2-phenylindole (DAPI; 2 μg/ml, Molecular Probes) was applied. After extensive washing, the sections were mounted, coverslipped and viewed by a fluorescence microscope and confocal laser-scanning microscopes (TCS-SPE and SP8, Leica Microsystems). Sections incubated without the primary antibodies were used to confirm they were free of immunofluorescence. Images were processed with Photoshop (CS3, 6, Adobe Systems) for the figures. Adjustments of brightness and contrast were equally applied across the entire images. Immunostaining with antibodies 2B6 and GluR2/3 were weakened considerably after fixation and decalcification. To avoid such attenuations, 2B6 was applied to the auditory nerves excised from the perfusion-fixed specimens without decalcification. However, in synaptic labelling with GluR2/3, we had no choice but to use fixed and decalcified samples. Both experimented and sham samples were processed at the same session.

### Sample collection for Western blotting, qRT-PCR and ELISA studies

We first traced the facial nerve that was situated antero-superior to the vestibulocochlear nerve from the internal auditory meatus (IAM) to the brainstem by inserting a nerve hook (No.10030-13, Fine Science Tools, Inc. Canada) between them and the facial nerve was entirely separated and removed. Next, the vestibular portions of the 8th cranial nerve were identified posterior to the auditory nerve and removed. With these procedures the auditory nerve was entirely observed from the IAM to the brainstem. On the brainstem, ventral/dorsal cochlear nuclei were recognized as a prominent tubercle and were peeled from the brainstem. Next, the nerve hook was inserted to the fundus of the internal auditory canal and the auditory nerve tissue was scraped out as much as possible. As a result, *en bloc* samples contained large cochlear nucleus tissue with small funnel-shaped auditory nerve/root without including tissue from other regions. These samples were used for quantification of glial scar formation in the cochlear nucleus and auditory nerve.

**Western blotting of GFAP**

Samples were collected from experimental rats, 4 weeks after compression (right side, n=19) and those from sham rats were used as control. Total protein was extracted by homogenizing and sonicating the tissue in RIPA buffer (Sigma). After centrifugation of the homogenate at 1,000×g and 4 °C, the supernatant was resolved in a buffered solution, consisting of SDS, Tris-HCl and proteinase inhibitor (Cell signaling) and boiled at 98°C for 2 min. after adding 2-mercaptoethanol. Proteins were separated on a SuperSep Ace gel (Wako) and subsequently transferred into PVDF membrane (GE Healthcare). Membranes were blocked for 1 hour in 5% BSA and probed with GFAP antibody (1:15,000, Dako, rabbit polyclonal) overnight. As the secondary antibody, horseradish peroxidase-linked anti-rabbit IgGs (1:10,000, GE Healthcare) were applied. Proteins were visualized with Amersham ECL Prime Western Blotting Detection Reagent (GE Healthcare) according to the manufacturer's instructions. Blots were also probed for GAPDH as a loading control. Single membrane simultaneously including lanes of injured and control samples and molecular size markers side-by-side were used for evaluation.

**qRT-PCR**

The samples were collected from the rats 1, 4, and 25 weeks after compression (15 rats for each time point) and immersed in ice cold solution of protease inhibitor/RIPA buffer and stored in liquid nitrogen until homogenization. The samples were collected in a solution with buffer RLT with 1% 2-mercaptoethanol and homogenized with a QIA shredder homogenizer (Qiagen). Total RNA was extracted by using an RNeasy Mini Kit (Qiagen). Prior to the reverse transcription reaction, potentially contaminating residual

genomic DNA was eliminated by Turbo DNase (Ambion). We used a High Capacity cDNA synthesis kit (Applied Biosystems) to synthesize single-stranded cDNA. The RT reaction conditions were as follows: 25 °C for 10 min, 37 °C for 120 min, 85 °C for 5 sec. Real-time PCR was performed using an ABI prism 7000 (Applied Biosystems). The PCR reaction sample was prepared as a mixture of 7.5ul of 2× Taqman Universal PCR Master mix (Applied Biosystems), 0.75ul of 20× Taqman Gene Expression Assays and 6.75ul of the properly diluted cDNA. The expression level of each gene was normalized with a control TaqMan probe (GAPDH). Real-time PCR primers and probes were obtained from Applied Biosystems (CSPG3, Neurocan, Rn00581331_m1; GFAP, Rn00566603_m1; Nestin, Rn00564394_m1). Amplification was performed with a program of 50 °C for 2 min, 95 °C for 10 min, followed by 40 cycles 95 °C for 15 sec, 60 °C for 1 min. The data were acquired in triplicate. Gene expression values, normalized to GAPDH expression, were determined by using the comparative Ct method (ΔΔCt method). The abundance of each transcript was expressed relative to the levels in auditory nerve/cochlear nucleus in sham rats.

**ELISA**

ELISA was performed by staff at MACROPHI Inc. (http://macrophi.co.jp/english/) who had no information about the categories of the samples. Samples collected from 30 rats (5-10 weeks after compression) and stored at −80 °C were quickly thawed and diluted to 1:10 w/v with the buffer containing 100mM Tris–HCl (pH 7.2), 400mM NaCl, 4mMEDTA, 0.05% sodium azide, 0.5% gelatin, 0.2% Triton-X 100, 2% BSA, and complete protease inhibitor cocktail. The samples were homogenized under ice-cold condition and the homogenates were centrifuged (11,000×g, 20min, 4 °C). The supernatant was collected and ELISA study was performed for quantification of endogenous BDNF with a Promega BDNF Emax ImmunoAssay System following the manufacturer's instructions. Briefly, 96-well immunoplates were coated with 100 µl/well of monoclonal anti-BDNF mouse antibody and incubated overnight at 4 °C. Non-specific binding was blocked with Block and Sample buffer. Then the samples and standards in duplicate were added to the coated wells (100 µl each) for 2 h at RT. After 2 h, the antigen was incubated with polyclonal anti-human BDNF antibody for 2 h at RT and then incubated with an anti-IgY HRP for 1 h at RT. The addition of 3,3',5,5'-tetramethylbenzidine started the colour reaction. The reaction was stopped 10 min later with 1M HCl solution, and the absorbance was immediately measured at 450 nm with correction between 750 nm (BIO RAD model 680 Microplate reader, Bio-Rad Laboratories).

## Legends for Supplementary Figures

**Figure S1. Techniques to induce glial scar in rat auditory system, to transplant donor cells to gliotic auditory nerve and the primary andibodies used in this study.** **(**A) Operative view of auditory nerve compression in the cerebellopontine angle (CPA). Red circle correspondes that in Fig. 1A. Fundus, fundus of the internal auditory canal; IAM, internal auditory meatus; PB, petrous bone. (B) Donor cells were transplanted to gliotic auditory nerve by two different techniques, intra-neural method (1) and surface transplatnation method (2). The tips of the syringe needles are indicated by circles. (C) Primary antibodies used to identify relevant endogenous and exogenous components of the auditory system (SI Methods).

**Figure S2. Neural generators of ABR and ABR waveform changes after surgical ablation of cochlear nucleus tissue and auditory nerve injury/subsequent glial scar formation.** (A) In small experimental animals including rat, wave I of ABR is generated from the auditory nerve and wave II, III, IV and V mainly reflect synaptic activities in the cochlear nucleus, superior olivary complex, lateral lemniscus and inferior colliculus, respectively. (B) Acute experiment to remove a part of the cochlear nucleus with a sucker depressed wave II and the following waves markedly while wave I maintained, confirming wave II was generated from the cochlear nucleus. Note the amplitude of wave I was not attenuated at this moment. (C) Normal configuration of ABR waveform was lost by auditory nerve mechanical injury and subsequent glial scar formation (dotted box in A). After compression, wave III was observed more apparently because of attenuation of wave II, the most prominent peak in small animal ABR. Measurements of wave III amplitudes and latencies are shown by blue perpendicular lines and red horizontal bi-directional arrows, respectively. Attenuation of wave I amplitude 5 weeks after auditory nerve injury was probably due to retrograde and Wallerian degenerations of auditory neurons. Anatomical figure cited from https://embryology.med.unsw.edu.au/embryology/index.php?title=File:Auditory_neural_pathway.jpg

# Figure S1

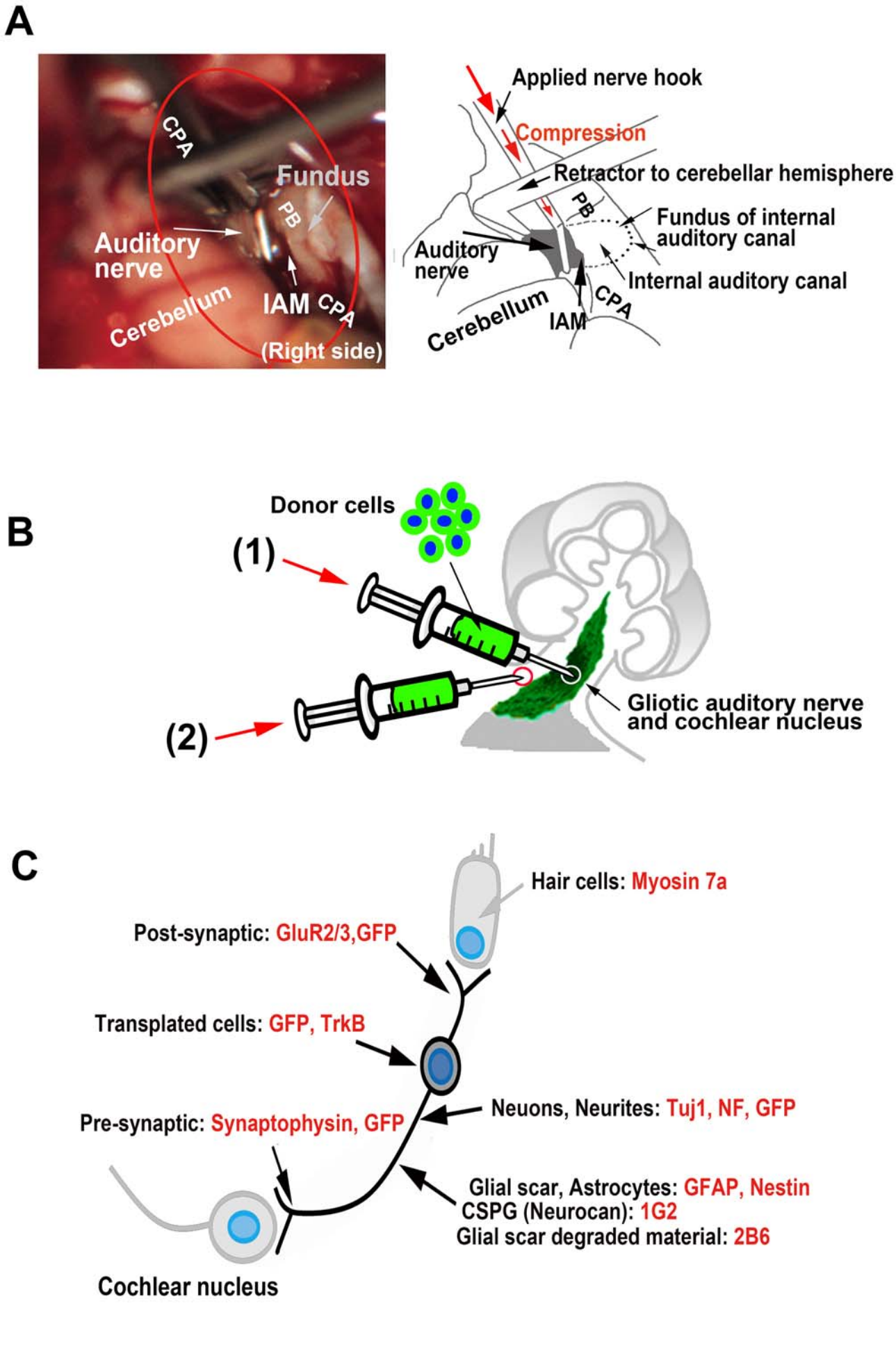

# Figure S2

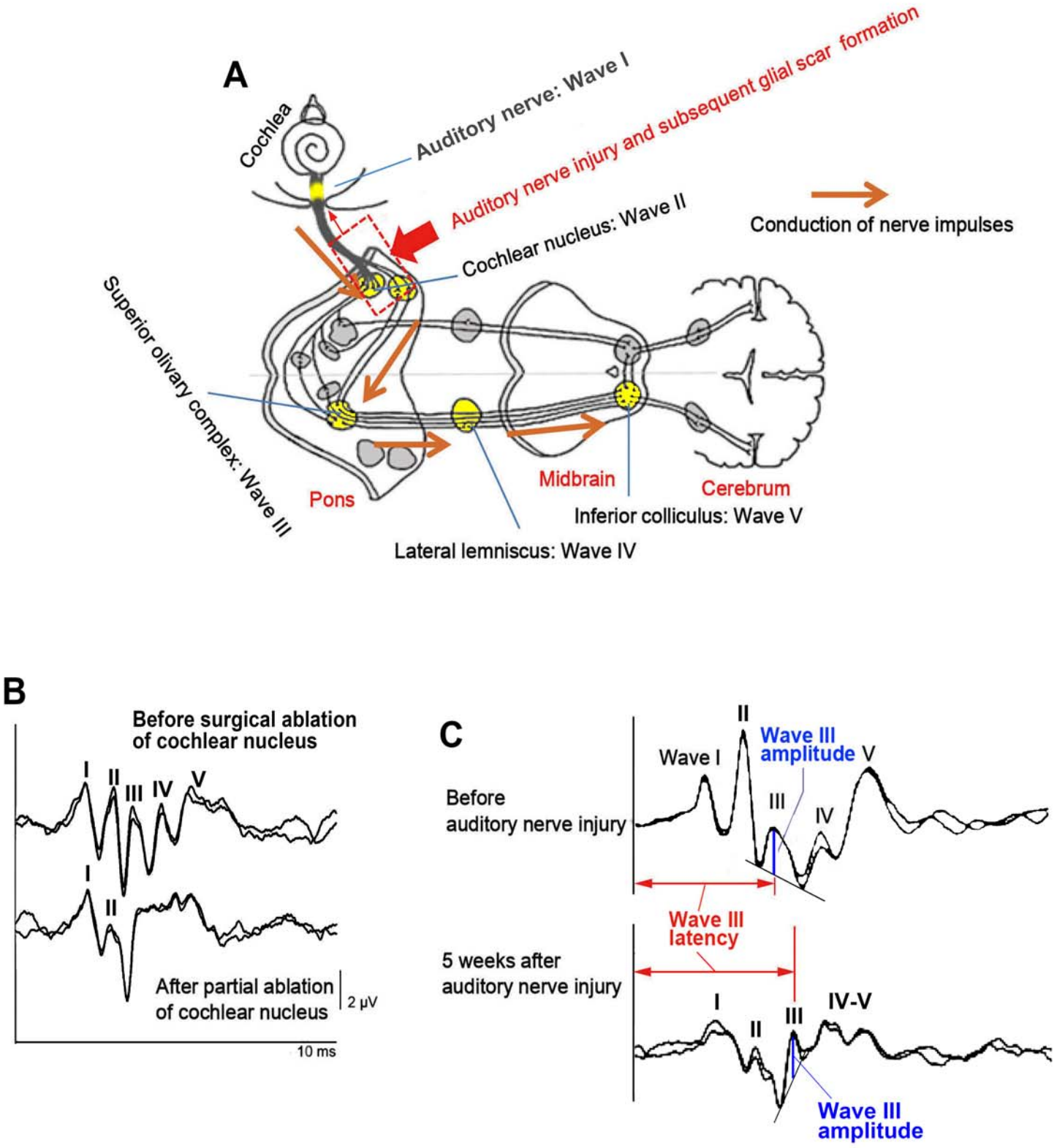

# Supplementary Table

## Table S1. Raw data of wave III amplitude (A), threshold (B) and latency (C) of 10 rats that demonstrated ABR improvement after cell transplantation

**(A)**

| Rat | | 1 | | 2 | | 3 | | 4 | | 5 | |
|---|---|---|---|---|---|---|---|---|---|---|---|
| Wave III amp (μV) | | Pre | Post | Pre | Post | Pre | Post | Pre | Post | Pre | Post |
| | 4 kHz | 1.146 | 3.014 | 2.446 | 3.467 | 0.840 | 3.310 | 1.598 | 1.673 | 1.210 | 3.032 |
| | 8 kHz | 1.043 | 5.124 | 2.783 | 4.892 | 2.561 | 4.438 | 2.170 | 2.556 | 3.373 | 6.661 |
| | 16 kHz | 0.452 | 2.883 | 2.174 | 3.273 | 1.428 | 2.533 | 0.964 | 1.174 | 2.476 | 3.574 |

| Rat | | 6 | | 7 | | 8 | | 9 | | 10 | |
|---|---|---|---|---|---|---|---|---|---|---|---|
| Wave III amp (μV) | | Pre | Post | Pre | Post | Pre | Post | Pre | Post | Pre | Post |
| | 4 kHz | 2.030 | 3.093 | 2.309 | 3.739 | 0.807 | 3.313 | 1.378 | 1.452 | 1.783 | 2.205 |
| | 8 kHz | 1.706 | 2.810 | 2.701 | 5.056 | 3.938 | 4.262 | 1.978 | 5.391 | 3.327 | 5.826 |
| | 16 kHz | 1.360 | 1.667 | 1.534 | 3.429 | 1.672 | 4.016 | 0.891 | 2.756 | 2.349 | 2.943 |

**(B)**

| Rat | | 1 | | 2 | | 3 | | 4 | | 5 | |
|---|---|---|---|---|---|---|---|---|---|---|---|
| Threshold (dB SPL) | | pre | post | pre | post | pre | post | pre | post | pre | post |
| | 4 kHz | 55 | 45 | 45 | 45 | 45 | 35 | 55 | 45 | 45 | 35 |
| | 8 kHz | 55 | 35 | 45 | 35 | 45 | 25 | 65 | 45 | 45 | 35 |
| | 16 kHz | 55 | 35 | 55 | 45 | 55 | 45 | 75 | 55 | 55 | 45 |

| Rat | | 6 | | 7 | | 8 | | 9 | | 10 | |
|---|---|---|---|---|---|---|---|---|---|---|---|
| Threshold (dB SPL) | | pre | post | pre | post | pre | post | pre | post | pre | post |
| | 4 kHz | 55 | 45 | 45 | 35 | 45 | 45 | 45 | 45 | 45 | 45 |
| | 8 kHz | 55 | 45 | 55 | 35 | 45 | 45 | 45 | 35 | 45 | 35 |
| | 16 kHz | 55 | 55 | 55 | 45 | 55 | 55 | 55 | 55 | 45 | 55 |

**(C)**

| Rat | | 1 | | 2 | | 3 | | 4 | | 5 | |
|---|---|---|---|---|---|---|---|---|---|---|---|
| | | Pre | Post | Pre | Post | Pre | Post | Pre | Post | Pre | Post |
| Wave III latency (ms) | 4 kHz | 4.075 | 4.050 | 4.100 | 3.950 | 3.950 | 4.075 | 4.050 | 4.025 | 4.100 | 4.075 |
| | 8 kHz | 4.175 | 4.075 | 4.150 | 4.100 | 5.675 | 5.675 | 4.125 | 4.025 | 4.100 | 4.125 |
| | 16 kHz | 4.175 | 4.150 | 4.300 | 4.200 | 4.200 | 4.200 | 4.400 | 4.150 | 4.225 | 4.225 |

| Rat | | 6 | | 7 | | 8 | | 9 | | 10 | |
|---|---|---|---|---|---|---|---|---|---|---|---|
| | | Pre | Post | Pre | Post | Pre | Post | Pre | Post | Pre | Post |
| Wave III latency (ms) | 4 kHz | 4.025 | 4.225 | 3.975 | 4.000 | 4.250 | 4.250 | 4.125 | 4.050 | 4.050 | 3.975 |
| | 8 kHz | 4.125 | 4.250 | 4.075 | 4.025 | 6.225 | 5.925 | 4.200 | 4.025 | 4.125 | 3.975 |
| | 16 kHz | 4.200 | 4.300 | 4.200 | 4.100 | 4.400 | 4.325 | 4.225 | 4.100 | 4.300 | 4.100 |

Amp, Amplitude; Pre, 5 weeks after auditory nerve compression and before cell transplantation; Post, 3 months after cell transplantation.